Macromolecular Materials and Engineering

Macromolecular Materials and Engineering Open Access

www.mame-journal.de

REVIEW OPEN ACCESS

Enhancing Crystallinity of Electrospun Polylactic Acid Fibers: Insights into Formation Mechanisms and Property Modulation–A Review

Kardo Khalid Abdullah[1] | Kolos Molnár[1,2,3]

[1]Department of Polymer Engineering, Faculty of Mechanical Engineering, Budapest University of Technology and Economics, Műegyetem Rkp. 3., BudapestH-1111, Hungary | [2]HUN-REN-BME Research Group for Composite Science and Technology, Budapest University of Technology and Economics, Műegyetem Rkp. 3., BudapestH-1111, Hungary | [3]MTA-BME Lendület Sustainable Polymers Research Group, Budapest University of Technology and Economics, Műegyetem Rkp. 3., BudapestH-1111, Hungary

Correspondence: Kolos Molnár (molnar@pt.bme.hu)

Received: 15 September 2025 | **Accepted:** 16 October 2025

Keywords: crystallinity | electrospinning | fibers | polylactic acid

ABSTRACT

Polylactic acid (PLA) electrospun fibers often lack sufficient crystallinity, which limits their mechanical strength, thermal stability, and functional performance. Tailoring a specific degree of crystallinity is therefore required for expanding the use of PLA fibers in various fields, where durability, degradation, and processability depend on controlled polymorphic phases. This review highlights recent studies on optimizing crystallinity by tuning electrospinning parameters to control fiber alignment and enhance molecular ordering. It also covers adding nucleating agents or fillers to lower crystallization barriers and using thermal or solvent annealing post-treatments to stabilize phases. Various additives have been demonstrated to modify the crystallinity of PLA electrospun fiber mats, influencing the balance between β-phase piezoelectricity, α' (metastable) and α (stable) phases, and $\alpha' \rightarrow \alpha$ phase transition during solvent evaporation. Scalable hybrid techniques and green processing approaches are emphasized to address sustainability concerns, while advances in real-time monitoring are highlighted as promising tools for achieving precise control over crystallization. This review synthesizes current knowledge to guide the design of PLA electrospun fibers with tailored crystallinity, balancing mechanical integrity, functional versatility, and environmental impact.

1 | Introduction

Natural and synthetic polymeric fibers have attracted considerable interest across academia and industry for their benign environmental footprint and excellent mechanical properties [1, 2]. Electrospinning (ES) has emerged as the leading method to produce micro- to nanoscale fibrous mats with precisely tunable porosity and morphology, yielding exceptionally high surface-area-to-volume ratios [3–5].

ES of bio-based polymers and biopolymers, including polylactic acid (PLA), poly(ε-caprolactone) (PCL), cellulose, and chitosan, offers the dual advantage of renewability and biodegradability, surpassing petroleum-derived materials in sustainability [6–9]. These materials facilitate the production of eco-friendly nanofibers with tunable mechanical, thermal, and biological properties. This versatility makes them suitable for biomedical applications, such as tissue engineering scaffolds, controlled drug delivery, and wound healing [10–14]. They are also promising materials for sustainable packaging and high-efficiency filtration systems [15, 16].

To compile the background for this review, a systematic literature search was conducted across Scopus, Web of Science, and

PubMed. Primary search terms included variations of polylactic acid (PLA, PLLA, PDLA) combined with ES-related terms (electrospun, ES) and crystallization-related terms (crystal, phase transition, annealing, stereocomplex). Publications were selected based on three main criteria. First, the study had to focus on PLA-based electrospun fibers. Second, it needed to analyze crystalline structure or phase behavior. Third, the study should report quantitative structure–property relationships. Studies were excluded if they lacked experimental validation. After screening and full-text assessment, around a hundred articles were retained. Approximately half of the selected studies were published between 2020 and 2025, reflecting recent advances and scalable methodologies. Roughly one-quarter appeared between 2015 and 2019, representing key foundational research on PLA phases. The remaining quarter was published before 2015, encompassing seminal works providing historical context.

PLA is a compostable thermoplastic polyester synthesized from renewable feedstocks such as sugarcane, maize, and cassava, combining high stiffness with excellent biocompatibility, enabling tailored performance across industrial and medical fields [17–20]. Despite these advantages, achieving controlled crystallinity in electrospun PLA remains challenging: rapid solvent evaporation and limited chain mobility during ES often trap the polymer in an amorphous state. Commonly employed solvents for ES PLA-based solutions include dichloromethane (DCM), chloroform ($CHCl_3$), dimethylformamide (DMF), hexafluoroisopropanol (HFIP), and 2,2,2-trifluoroethanol (TFE) [21]. The rapid evaporation of solvents during ES restricts the molecular mobility of PLA chains, forming kinetically trapped amorphous structures. Additionally, residual or entrapped solvents can further hinder chain rearrangement, thereby postponing crystallization [22, 23]. This kinetic arrest stems from insufficient time for PLA chains to undergo conformational rearrangements, resulting in a predominance of disordered molecular arrangements [24]. Consequently, the restricted chain alignment manifests as morphological defects, including voids and misoriented crystallites, which deteriorate mechanical performance by reducing Young's modulus and tensile strength. These combined effects limit their utility in load-bearing biomedical meshes or high-temperature filtration membranes applications. Furthermore, the amorphous domains accelerate hydrolytic degradation rates with higher water diffusion rates [25].

Despite considerable advances in enhancing the crystallinity of electrospun PLA fibers, current strategies often address only isolated aspects without considering the interplay of polymorphic phases, processing kinetics, and scalability. Many studies focus narrowly on individual aspects—like tuning ES parameters or adding nucleating agents—without addressing the broader trade-offs among mechanical performance, biodegradation, and manufacturability. For example, β-phase crystallinity, promoted by high elongational stress, enhances piezoelectricity and tensile strength yet compromises long-term stability, and thermal annealing increases α-phase content at the cost of energy-intensive steps unsuitable for mass production [26–28].

In this review, we explore how precise control of PLA's crystalline phases ($\alpha' \rightarrow \alpha$, β, γ, and stereocomplex) influences mechanical strength, piezoelectricity, thermal resistance, and degradation. We also highlight the effects of rapid ES kinetics, including jet stretching and solvent evaporation, on these properties. Furthermore, it is proposed that nanofiber crystallinity and functionality can be optimized by tuning solution and processing parameters, incorporating nucleating agents or enantiomeric blends, and applying targeted post-treatments. The effectiveness of these strategies can be further improved through real-time in situ monitoring and data-driven feedback. This approach bridges the gap between laboratory investigations and sustainable, industrial-scale production of high-performance PLA nanofibers.

2 | Crystalline Properties of PLA

2.1 | Crystalline Phases

The semi-crystalline morphology of PLA is governed by the folding and stacking of polymer chains into ordered lamellar structures [29, 30]. In contrast, amorphous domains are mainly characterized by disordered chain configurations, which influence the dimensional stability [31].

PLA comprises polymerized lactic acid units, originating from L-lactide, D-lactide, or a mixture of both enantiomers. A commercial L-lactide-based polymer (PLLA) normally contains 1%–2% D-lactide content, and vice versa with a D-lactide-based (PDLA) polymer. Incorporating enantiomers introduces stereochemical defects within the chain, disrupting lamellar stacking and prolonging nucleation induction periods. For instance, semi-crystalline PLLA grades containing ~2 wt.% D-lactide comonomer exhibits markedly retarded crystallization rates. This slowdown occurs because these defects hinder the formation of α-phase crystallites. The phenomenon is attributed to lattice distortion and reduced fold-surface regularity [32]. This enantiomer-dependent crystallization suppression underscores the delicate balance between PLA systems' chain dynamics, stereoregularity, and crystalline perfection.

On the other hand, stereocomplex PLA is composed of a 50:50 mixture of the enantiomers, and the neighboring molecules are interlocking in a highly regular, tightly packed structure, like a zip lock. This results in improved crystallinity, better mechanical performance, and a significantly higher melting temperature of such lamellae [33, 34]. The stereocomplex crystals, with a melting temperature of 230°C, make the material suitable for heat-resistant applications [34].

The crystallinity of semi-crystalline polymers is often modeled by the classical three-phase model, which also applies to various PLA materials. This considers that besides the crystalline phase, a rigid and a mobile amorphous phase exists, which behaves fundamentally differently [35–37]. Positioned at crystalline-amorphous interfacial regions, the rigid amorphous fractions (RAF) arise from constrained chain segments that partially align with adjacent crystallites, creating a gradient in molecular packing density [37]. On the other hand, the mobile amorphous phase (MAF) is soft and flexible because the surrounding crystalline domains do not hinder conformational changes [38]. The RAF is immobile, but still significantly modulates viscoelastic behavior by acting as a stress-transfer mediator between crystalline and MAF phases, enhancing fracture toughness while maintaining glass

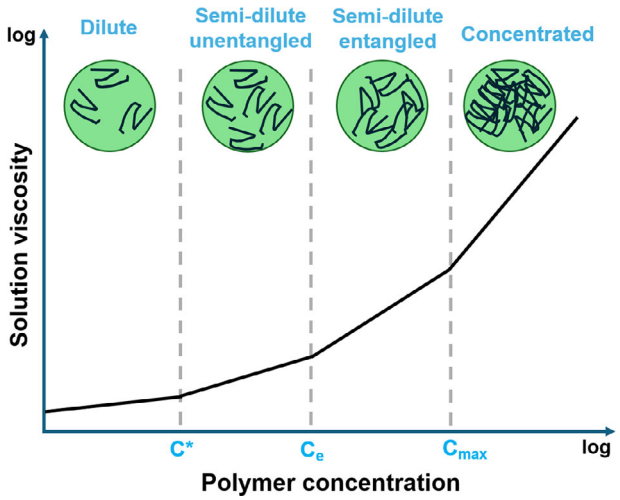

FIGURE 1 | Concentration-dependent regimes of polymer solutions relevant to ES. Green circles represent the solvent medium, and black lines represent polymer chains. Adapted with permission from [44]. Copyright (2020), Elsevier.

transition-associated flexibility [39]. The interplay between these three phases (crystalline, MAF, and RAF) governs the overall thermomechanical behavior of PLA by restricting polymer chain mobility.

The crystallization kinetics of PLA are critically influenced by its molecular weight and stereochemical purity [40]. The molecular weight threshold for stable entanglements is estimated to be between 13 and 28 kg/mol [41]. High-molecular-weight PLA generally shows suppressed crystallization due to more chain entanglements per molecule that restrict segmental mobility. Conversely, at low molecular weights, PLA fails to form fibers due to insufficient chain entanglements to stabilize jet stretching [42]. If crystallization is done from a solution (such as at ES), the solution concentration becomes a key factor. Below a critical concentration, no fibers can be spun since, again, a stable, entangled structure is required to form fibers.

ES from solutions within entanglement concentration allows significant jet deformation and molecular alignment [43]. This alignment, driven by slow polymer relaxation and low solution viscosity, enhances cold crystallization rates of fabricated fibers. The polymer concentration and viscosity relationship can be divided into four distinct regimes, each influencing fiber formation and crystallization, as shown in Figure 1.

The solution is too diluted for fiber formation below the overlap concentration (c*), leading to electrospraying or bead formation with negligible crystallinity. Between c* and the entanglement concentration (c_e), in the semi-dilute unentangled regime, polymer chains begin to overlap. This allows partial jet stretching and molecular alignment, which enhances cold crystallization potential, even though beads or spindle defects may still appear in the fiber morphology [45]. As polymer concentration increases beyond the critical entanglement threshold (c_e) and enters the mid-range of the semi-dilute entangled regime, sufficient viscoelasticity enables stable jet formation, uniform fiber morphology, and enhanced chain orientation, collectively promoting improved intrinsic crystallinity. However, as concentration approaches the maximum spinnable threshold (c_{max}), excessive viscosity restricts jet stretching and solvent evaporation, potentially leading to heterogeneous or suppressed crystallization despite high chain density. Thus, the degree of crystallinity in electrospun PLA mats is closely tied to solution concentration and viscoelastic behavior, with an optimal window above c_e and below c_{max}.

PLA exhibits polymorphic crystallization behavior, manifesting in several primary crystalline phases (α, β, γ) with distinct chain conformations and lattice configurations, as shown in Figure 2. The thermodynamically stable α-phase, characterized by De Santis and Kovacs [46], forms under conventional melt- or solution-crystallization conditions. It adopts a 10_3 helical conformation arranged in an orthorhombic unit cell, with characteristic X-ray diffraction (XRD) reflections at $2\theta = 14.8°$, 16.9°, 19.1°, and 22.5° [47]. This α-phase structure arises from the regular packing of alternating upward (U) and downward (D) 10_3 helices [48]. During non-isothermal crystallization, the metastable α'-phase (disordered analog of α) dominates below 100°C, featuring looser chain packing and reduced interlamellar cohesion. Abovhinrmally activated chain reorganization drives α'-to-α transition via progressive helical ordering and lamellar thickening [49]. At such a temperature, crystal perfection and lamellae's thickening also occur in parallel to the reorganization [50, 51].

The strained β-phase, induced under high-strain conditions (e.g., fiber drawing at elevated temperatures), stabilizes a 3_1 helical conformation within an orthorhombic unit cell [53]. Notably, the α-to-β transition involves a fundamental reorganization of chain packing. Wang et al. [54] demonstrated that U and D helices in the α-phase lattice slip along (110) crystallographic planes under mechanical strain. This slippage progressively disorders the original helical arrangement, ultimately yielding the β-phase with an alternating U/D 3_1 helix configuration [55]. Alongside, stretching drives conformational evolution from the 10_3 helix (α-phase) to the compressed 3_1 helix (β-phase), enabling non-centrosymmetric alignment that results in piezoelectricity, a key feature for electromechanical applications [56].

Beyond the α and β polymorphs, PLA also forms γ-phase, typically epitaxially grown on hexamethylbenzene substrates at ~140°C, features a 3/1 helical symmetry with three monomeric units per helical turn [47, 57]. Despite its structural novelty, γ-phase instability and substrate dependency limit practical utility. Finally, the δ-phase remains poorly characterized, with conflicting reports about its existence as a distinct polymorph versus a disordered intermediate.

While the homopolymer phases of PLA each exhibit distinct structural features, they are limited in thermal stability and mechanical performance. Stereocomplex PLA (sc-PLA) has emerged as a more robust crystalline form to overcome these issues. When equal amounts of PLLA and PDLA are combined, their enantiomeric chains interlock through strong intermolecular and hydrogen-bonding interactions, creating a tightly packed co-crystalline structure like a molecular "zip-lock." These stereocomplex crystals melt at approximately 220°C–230°C—about 50°C higher than PLA homocrystals—and outperform in

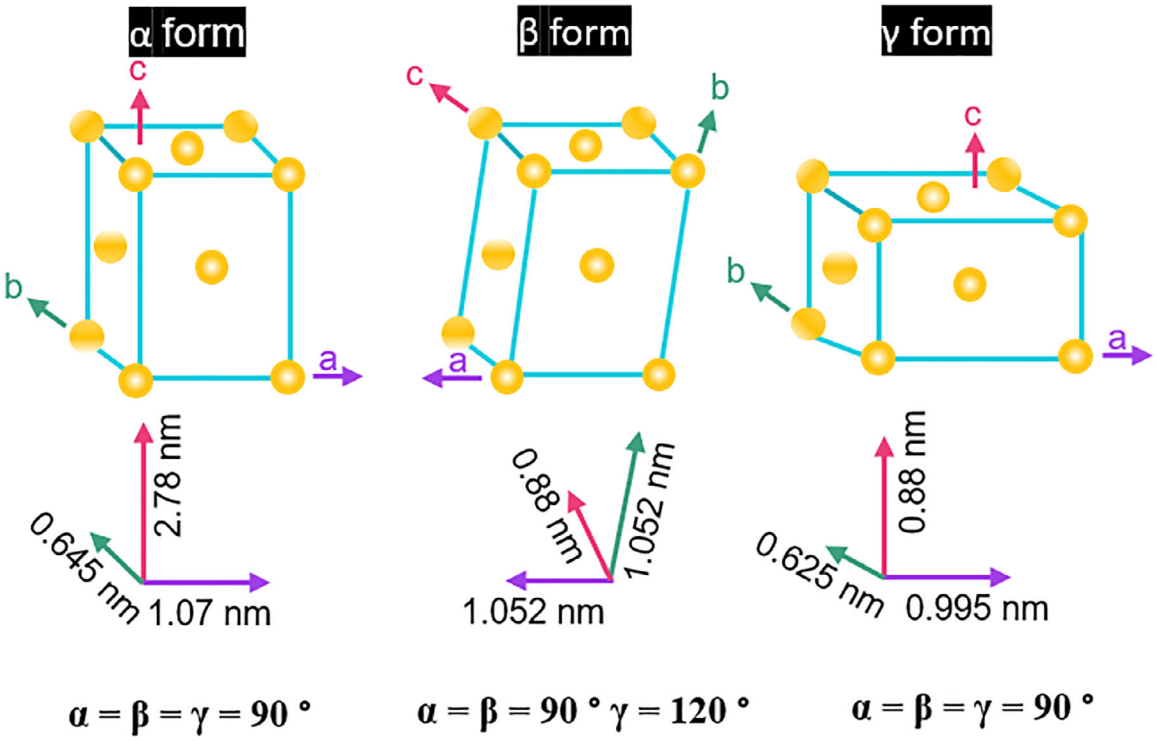

FIGURE 2 | The crystal configurations of α, β, and γ phases of PLA. This figure is adapted from [52] under the Creative Commons Attribution 4.0 International License (CC BY 4.0).

mechanical strength, thermal resilience, and hydrolytic stability [58]. In the context of electrospun fibers, sc-PLA formation offers significant advantages. ES equimolar PLLA/PDLA solutions selectively promote stereocomplex crystallites while suppressing homocrystallinity, resulting in fibers with enhanced modulus and higher crystallinity [59–61]. Beyond kinetic limitations, the stereochemical composition of PLA further complicates crystallization during ES. Each 1% increase in D-lactide content reduces the melting temperature (T_m) by ~5°C [26], destabilizing crystalline domains through stereochemical defects that form lattice strain. A comprehensive comparison of these phases, including their structural and thermal attributes, is presented in Table 1.

Advancements in analytical and processing technologies have enabled precise manipulation and characterization of PLA's crystallization mechanisms, directly addressing the phase-specific challenges. Terahertz time-domain spectroscopy (THz-TDS) now permits in situ monitoring of sub-picosecond conformational transitions during α'-to-α phase evolution, resolving helical ordering dynamics [66, 67]. This capability aligns with recent thermally activated chain reorganization findings, providing mechanistic insights into the disordered-to-ordered structural progression.

Complementing these analytical advances, high-pressure processing (HPP) at 300 MPa/185°C has been demonstrated to increase PLA crystallinity to 66.3% [68]. This breakthrough is particularly relevant for high-molecular-weight systems, where dense chain entanglements usually hinder crystallization. By compressing free volume and promoting homogeneous nucleation, HPP overcomes kinetic barriers to chain alignment, effectively decoupling crystallinity. These synergistic developments in characterization and processing underscore a paradigm shift toward predictive crystallinity control in PLA systems, bridging the gap between polymorphic behavior and application-specific performance requirements.

At typical processing conditions from a solution or melt, typically α' and α crystals are formed. When stretching, β crystals might also be present, although uncommon. If PDLA and PLLA are mixed, stereocomplex crystals can also be easily generated.

2.2 | Crystallization Mechanisms and Structural Evolution

The ES process imposes kinetic constraints on PLA, favoring uniaxial fiber orientation at the expense of long-range crystalline order. Rapid solvent volatilization (10^{-2}–10^{-3} s) and ambient processing temperatures (typically 20°C–30°C) restrict segmental mobility, resulting in metastable structures dominated by amorphous domains and kinetically trapped α'-phase crystallites. This contrasts with thermally processed PLA, where controlled cooling rates (10^{-1}–10^{2}°C/min) enable progressive lamellar thickening and α-phase stabilization through helical conformation annealing. In this process, disordered α' helices reorganize into the stable 10_3 α-helix [69]. Additionally, fold-surface regularization heals misfolds at lamellar interfaces, reducing defect density and promoting stable crystal growth [70]. Although the elongational flow in the ES jet aligns chains axially, the absence of sufficient relaxation time precludes these defect-mitigation steps [69]. Consequently, post-ES isothermal annealing at 80°C–120°C is required to restore segmental mobility. This restored mobility

TABLE 1 | Summary of PLA crystalline forms, including lattice characteristics, formation conditions, and relative melting temperatures.

Crystalline form	Description	Formation conditions	Lattice type	Lattice parameters (a/b/c)	Melting temperature (°C)	References
α	Most stable, highly ordered	Slow cooling or annealing above ~120°C	Orthorhombic	1.07 nm/0.65 nm / 2.78 nm	170–180	[50, 62]
α'	Disordered, less stable	Crystallization below ~100–120°C	Pseudo-orthorhombic (disordered)	1.07 nm/ 0.61 nm/ 2.88 nm	150–160	[50, 63]
β	Rare, metastable form	Uniaxial drawing at high strain rates	Trigonal or pseudo-hexagonal	1.05 nm / 1.05 nm / 0.88 nm	180–190 (unstable)	[50, 51, 64]
γ	Very rare	Epitaxial crystallization on certain substrates (e.g., hexamethylbenzene)	Orthorhombic (two antiparallel 3_1 helices)	0.99nm / 0.63 nm / 0.88nm	~165	[65]
Stereocomplex (sc-PLA)	Complex of PLLA and PDLA (1:1)	Co-crystallization of high-mol. wt. PLLA + PDLA	Triclinic	0.916 nm / 0.916 nm / 0.870 nm, $\gamma \approx 109.2°$	~230	[58]

enables reverse chain reptation, which is the back-diffusion of chain segments out of misfolded regions. As a result, the $\alpha' \rightarrow \alpha$ transition occurs, accompanied by lamellar thickening and defect healing.

Achieving uniform crystallization in electrospun PLA mats is intrinsically difficult because variations in solution viscosity, ambient humidity, and electric-field strength produce spatially heterogeneous fiber morphologies and nucleation sites. Since significant crystallization in PLA fibers occurs predominantly during post-spinning thermal treatment rather than in the millisecond drying window, researchers have turned to in situ (i.e., real-time) spectroscopic monitoring during isothermal annealing. Techniques such as Raman spectroscopy and ATR-FTIR can track the growth of α-phase peaks and the decay of amorphous signatures as the mat is held at 80°C–120°C. This enables closed-loop control of annealing time and temperature to minimize structural heterogeneity [71, 72]. As a result, both crystallinity and mechanical integrity can be optimized.

2.3 | Relationship Between Crystallinity and Physical Properties

Electrospun (PLA) fibers exhibit a complex semicrystalline architecture that fundamentally dictates their mechanical behavior. This morphology arises from the interplay between crystalline lamellae, RAF, and MAF, each contributing distinct functionalities. Crystalline lamellae act as nanoscale reinforcing "backbones" that resist plastic deformation through steric constraints on chain displacement [73, 74]. Their lamellar thickness and stacking density directly govern tensile modulus and yield strength, as thicker lamellae impede dislocation motion more effectively. The MAF facilitates viscoelastic energy dissipation via segmental chain mobility, enabling ductility and impact resistance. RAF enhances stiffness by acting as physical crosslinks but suppresses large-scale chain slippage, reducing fracture toughness. However, the RAF could not contribute to the heat fusion of crystal melting but could affect the glass transition and the stability of the polymer molecular chains [75, 76].

RAF expands at the expense of the MAF, driving a transition from ductile to brittle behavior. For instance, electrospun PLA mats with 8.5% crystallinity exhibit a yield strength of 10.93 MPa, whereas raising crystallinity to 16.2% nearly doubles it to 21.9 MPa [77]. This nearly two-fold strength gain reflects the greater density of rigid crystalline domains that restrict chain motion under stress. This strengthening arises from the percolation of rigid crystalline domains that restrict chain mobility under stress, while the diminished MAF fraction limits energy dissipation pathways. Notably, the RAF/MAF ratio provides greater predictive power for toughness than crystallinity alone, as it quantifies the balance between energy dissipation and crack propagation resistance.

Moreover, elongational flow during ES can promote axial chain alignment and potentially enhance in situ crystallinity and mechanical strength. Still, the ultrafast solvent evaporation (10^{-2}–10^{-3} s) and low processing temperature typically trap PLA in the metastable α'-phase. Only through post-spinning treatments, such as isothermal annealing, can the fibers undergo the $\alpha' \rightarrow \alpha$

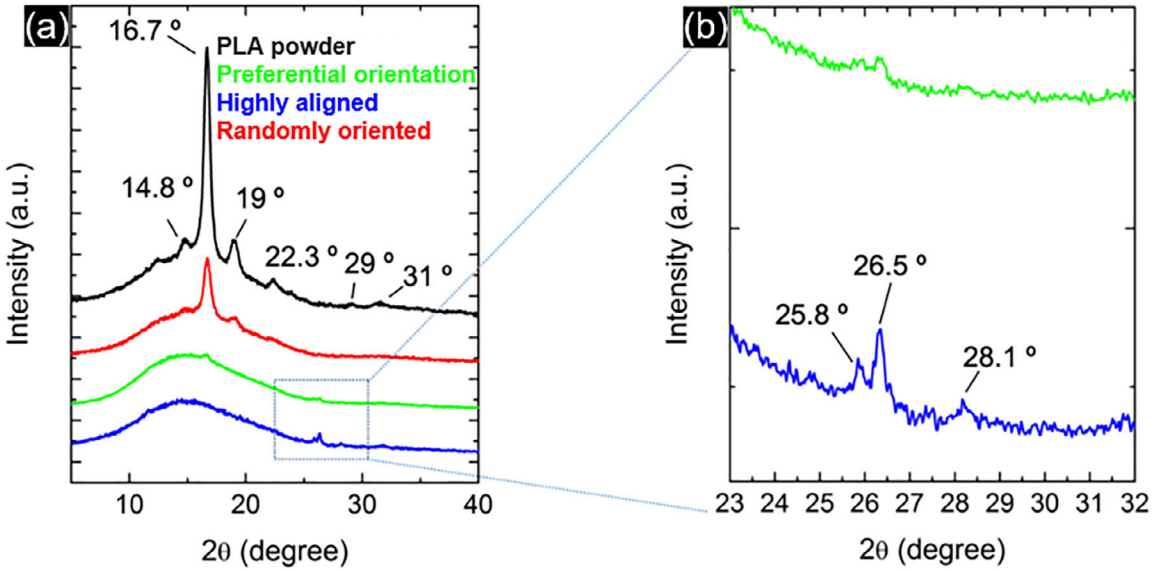

FIGURE 3 | (a) X-ray diffraction patterns for PLA powder, randomly oriented, partially oriented, and highly oriented PLA fibers. (b) Zoomed-in section of the 2θ range between 23° and 32°, highlighting the β-phase region of highly aligned and preferentially oriented fibers. This figure is adapted from [26] under the Creative Commons Attribution 4.0 International License (CC BY 4.0).

transformation, achieve more uniform crystalline order, and realize the full mechanical benefits of the α-phase.

Beyond mechanical performance, crystallinity significantly affects PLA's optical and barrier properties. Amorphous PLA is optically transparent (haze <10%), while semicrystalline counterparts with >30% crystallinity exhibit increased opacity (haze >70%) due to the formation of spherulites larger than the wavelength of visible light (~400–700 nm). This transition has functional implications: while transparency is favored in packaging applications (e.g., visual inspection windows), increased haze may be advantageous in UV-blocking agricultural films. Additionally, crystalline domains serve as barriers to gas diffusion, increasing tortuosity and impeding permeation compared to more permeable amorphous regions [78]. Electrospun fibers often maintain higher optical transparency (lower haze) and exhibit greater gas permeability, due to reduced chain ordering and inter-fiber porosity.

2.4 | Influence of Crystalline Structure on the Degradation Behavior

Crystallinity influences the degradation kinetics of PLA fibers, especially in electrospun mats where fiber morphology and crystallite distribution diverge from those of bulk materials. The spatial arrangement of crystalline and amorphous phases governs PLA degradation pathways—hydrolysis, photolysis, thermolysis, and enzymatic cleavage—each proceeding at distinct rates depending on the underlying microstructure [79].

Amorphous regions, particularly the MAF, are more susceptible to hydrolytic attack due to enhanced water uptake and chain mobility. As these domains erode, residual polymer chains can reorganize into crystalline α-phase, transiently elevating overall crystallinity. For instance, immersion in phosphate-buffered saline (PBS) induces preferential degradation of amorphous domains, yielding a temporary rise in crystallinity [80]. Comparable behavior has been observed in wet-spun PLA fibers, where hydrothermal degradation facilitates microcrystalline $\alpha' \rightarrow \alpha$ transformation [81]. With extended exposure, even crystalline regions succumb to hydrolysis: early-formed microcrystals in wet-spun fibers eventually degrade, underscoring the inherent vulnerability of crystalline domains. In electrospun PLA fiber mats, prolonged hydrolytic exposure yields a gradual decline in crystallinity concomitant with continuous mass loss, indicating progressive breakdown of both amorphous and crystalline structures [77].

Photodegradation of electrospun PLA fibers is likewise dictated by crystalline architecture: ultraviolet radiation preferentially targets disordered (amorphous) regions, where the MAF absorbs UV light and generates free radicals that instigate chain scission [82]. In contrast, well-developed α-phase crystallites confer superior UV shielding through enhanced reflectivity and structural perfection. Under thermo-oxidative conditions, crystalline domains and the rigid amorphous fraction (RAF) in bulk PLA act as diffusion barriers to oxygen ingress, thereby elevating the activation energy for thermal decomposition [83]; however, this mechanism remains poorly understood in the context of electrospun PLA fibers.

3 | Crystallinity Advancements

3.1 | Tuning ES Parameters to Control Crystallinity and Polymorphism

The crystallinity and polymorphic behavior of PLA electrospun fibers are governed by ES parameters that regulate chain entanglement dynamics, nucleation kinetics, and stress-induced phase transitions. Key variables include polymer solution concentra-

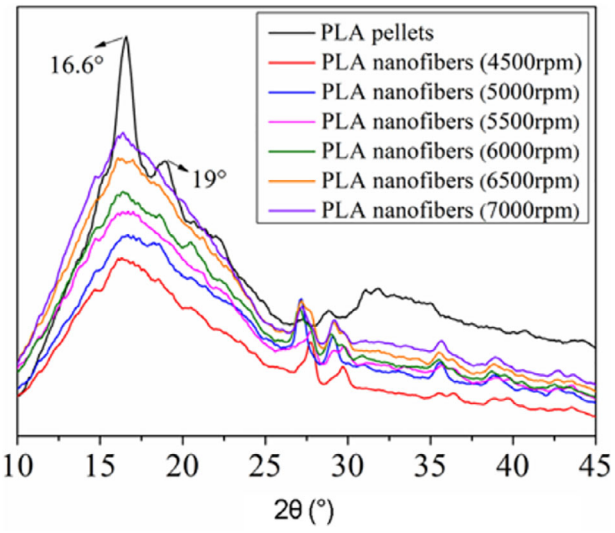

FIGURE 4 | XRD patterns of PLA pellets and electrospun fibers collected at various rotational speeds of the collector. Reproduced with permission from [85]. Copyright (2020), Springer Nature.

tion, electric field strength, feed rate, and collector geometry/kinematics (e.g., rotational velocity, patterning). Each of these factors individually and collectively influences fiber morphology and the organization of the crystalline domain.

Solution concentration strongly affects PLA fiber crystallinity, but its impact is non-linear and depends on polymer molecular weight, stereochemistry, and solvent system. Higher concentrations generally increase chain entanglement, facilitating α-phase packing, while very low concentrations may produce insufficient chain overlap, reducing crystallinity. For instance, studies comparing 6 and 10 wt.% PLA solutions (with all other parameters constant) report a marked increase in crystallinity with the higher concentration [77]. These trends illustrate that solution concentration primarily governs the overall molecular ordering during ES.

Electric field strength and feed rate control elongational stresses in the polymer jet, which influence polymorphic transitions. Higher field strengths and slower feed rates increase chain stretching, promoting alignment into the 3_1 helical conformation characteristics of mechanically robust β-phase domains [78]. For example, a 5 wt.% PLA solution electrospun at 15 kV and 12.5 cm needle-to-collector distance produced fibers with 46.6% crystallinity, whereas higher field strength (25 kV) and 15 cm distance reduced crystallinity to 26.2% [84]. These examples demonstrate the competing influences of elongational strain versus chain entanglement in determining the α/β-phase ratio.

Strain-induced crystallization is strongly affected by collector motion. Dynamic collector systems, such as rotating drums (1300–3000 rpm), induce uniaxial fiber alignment and shear-induced crystallization, which can facilitate β-phase formation. Echeverría et al. [26] used XRD to compare PLA powder with electrospun fibers of varying alignment. The PLA powder exhibited characteristic α-phase peaks at 16.7° and 19.1° (Figure 3a). Whereas, partially aligned fibers showed attenuated α-phase signals alongside emerging β-phase peaks at 25.8°, 26.5°, and 28.1° (Figure 3b), attributed to the β phase. However, these β-phase peaks are often subtle and may overlap with other features, making definitive assignment challenging without complementary methods (e.g., polarized FTIR, wide-angle X-ray scattering).

The impact of collector speed on fiber alignment and crystallinity has been further elucidated in recent studies. For instance, Xia et al. [85] reported that crystallinity increases with collector rotational speed (4500–7000 rpm), as shown in Figure 4. High rotational speeds consistently correlate with greater chain alignment and increased β-phase signatures, but at the expense of fiber uniformity beyond a critical rpm. This indicates a trade-off between phase control and morphological homogeneity that must be optimized for application-specific requirements.

Higher collector speeds promote crystallization and enhance β-phase content in electrospun PLA fibers. A comprehensive summary of parameter-crystallinity relationships in ES is provided in [86], which we recommend for further reading.

3.2 | Additive Incorporation and Post-Processing Treatments

Two primary approaches modulate PLA crystallization behavior: additive incorporation into the polymer solution and post-processing treatments of fabricated fiber mats. Both methods influence nucleation density, phase selection, and lamellar organization, thereby dictating the final microstructure and functionality of the fiber mats. It is important to distinguish effects observed specifically in electrospun PLA fibers from those seen in PLA processed by other methods, such as melt extrusion or solution casting. This is because the ES process can drastically alter additive behavior with its rapid solvent evaporation and high strain rates.

3.2.1 | Additives in ES Solutions

Inorganic nanoparticles, such as hydroxyapatite and montmorillonite, act as heterogeneous nucleation agents by lowering the activation energy required to initiate crystal growth. These high-surface-area particulates facilitate lamellar stacking, promoting ordered crystal structures [87, 88]. For example, cellulose nanocrystals (CNCs), as investigated by Leonés et al. [89] in PLA (NatureWorks 3051D) electrospun from dimethylformamide/acetone, increased fiber crystallinity from ~9.4% to ~12.3% through epitaxial α-phase nucleation—demonstrating their ability to template ordered regions during rapid solidification. However, excessive CNC loading (>5 wt.%) led to nanoparticle aggregation, adversely affecting fiber continuity and mechanical uniformity. Low loadings (≈1–2 wt.%) of well-dispersed CNCs provide ES's most consistent α-phase enhancement; above a dispersion limit, aggregation dominates and negates benefits. Similarly, natural silicate-based additives such as diatomite have been shown to promote α-phase crystallization through surface-induced alignment of PLA chains. High surface area and favorable surface chemistry enhance templated lamellar arrangements, but dispersion quality is a dominant factor for reproducibility [90].

TABLE 2 | Additives and nucleating agents for modifying crystallinity in PLA electrospun fiber mats.

Additive category	Specific agent	Optimal loading	Key effects on PLA electrospun fibers	Crystal phase promotion	References
Inorganic nanoparticles	Cellulose nanocrystals (CNCs)	1–2 wt.%	↑ Crystallinity from 9.4% → 12.3%; epitaxial α-phase nucleation; >5 wt.% causes aggregation → fiber defects	α-phase	[89, 93, 94]
	Talc	3–6 wt.%	↑ Crystallization temp. by 16°C; ↑ nucleation density 500×; stable reference agent	α-phase	[52, 93, 94]
	Graphene oxide (GO)	0.5–1 wt.%	↑ Crystallinity to 49%; forms spindle-like nanopores (100–200 nm); >0.5 wt.% restricts crystal growth	α-phase	[47, 95]
	Diatomite	2–4 wt.%	Facilitating the formation of α-phase crystals and thereby enhancing the crystallinity	α-phase	[90]
Biomass-derived agents	Lignin	2–4 wt.%	Crystallinity increases by approximately 4% with the addition of 0.75 wt.% lignin to PLA	α-phase	[91, 96, 97]
	Chitin/Chitosan	3–5 wt.%	↑ Crystallinity to 4%; ↓ half-crystallization time ($t_1/_2$) from 92.7 → 1.4 min; enhances chain mobility	α-phase	[89, 98]
Stereocomplex agents	PDLA	5–10 wt.%	Forms stereocomplex crystallites; ↑ Tm by 50°C; ↑ crystallinity and heat resistance; dual-phase system with PLLA	SC crystallites	[33, 61, 94]
	Cyclic PLLA	1–3 wt.%	Unique topology ↑ nucleation efficiency; biocompatible; ↑ crystallinity from 21% → 48%	α-phase	[33, 61]

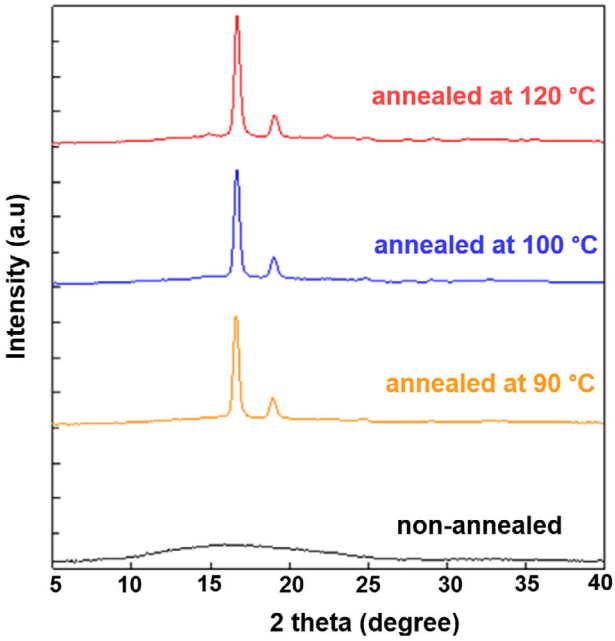

FIGURE 5 | XRD patterns of electrospun PLLA fiber mats in the non-annealed state and after annealing at 90, 100, and 120°C. This figure is adapted from [100] under the Creative Commons Attribution 4.0 International License (CC BY 4.0).

3.2.2 | Additives in General PLA Systems

Beyond ES, CNCs and similar additives have also been shown to enhance PLA crystallinity and mechanical properties in solution-cast films and melt-blended composites. However, the magnitude of crystallinity increases, and dispersion quality strongly depends on processing conditions and polymer grade. Likewise, the nucleation effect of diatomite and other silicate fillers in PLA composites varies with filler dispersion and interaction with the polymer matrix, making the impact less consistent outside ES [91]. However, lignin's intrinsic hydrophobicity often leads to phase separation, which may necessitate compatibilizers (e.g., maleic anhydride-grafted PLA) to maintain interfacial cohesion and prevent mechanical deterioration. Biopolymer additives such as lignin can increase nucleation density through π–π stacking with PLA ester groups. Still, hydrophobicity-induced phase separation often requires compatibilizers (e.g., maleic anhydride-grafted PLA) to maintain mechanical integrity.

Plasticizer agents such as PCL influence crystallization by improving chain mobility and lowering the glass transition temperature (T_g). In PLA/PCL blends (70:30 w/w), semi-crystalline PCL domains (45–50%) act as templates for PLA nucleation, yielding a dual-phase crystalline system. However, this comes at the expense of thermal stability, which decreases by approximately 10°C [92]. Inorganic salts such as NaCl and LiCl can also contribute to crystallization by increasing solution conductivity and promoting jet stretching during ES. Their ion–dipole interactions are hypothesized to facilitate β-phase nucleation. Moreover, certain metal salts (e.g., zinc acetate, calcium chloride) have been shown to significantly enhance PLA crystallinity by acting as heterogeneous nucleating agents. This effect, however, has been primarily demonstrated in bulk samples; in electrospun fibers, rapid solvent evaporation and fast solidification limit molecular rearrangement, thereby hindering crystal growth [93]. A comprehensive summary of additives and nucleating agents influencing the crystallinity of PLA electrospun fiber mats is presented in Table 2.

Additives primarily influence nucleation density and early-stage ordering, whereas post-processing governs lamellar thickening and phase equilibration. A two-stage strategy—(1) targeted additive templating during ES to partially initiate polymorph selection and (2) controlled post-annealing to promote lamellar growth—appears most promising for achieving high, reproducible α-phase content while retaining process throughput.

3.2.3 | Post-Processing Treatments (Applicable to ES and Non-ES PLA)

Post-processing treatments provide alternative routes to enhance PLA fiber crystallinity through thermomechanical or solvent-induced chain reorganization. Isothermal annealing of electrospun mats at sub-melting temperatures (≈80–120°C) facilitates enthalpic relaxation and promotes the α'-to-α phase transition by lamellar thickening. This change is typically observed as a small exothermic peak in differential scanning calorimetry (DSC) just below T_m [99]. Cuong et al. [100] subjected electrospun PLLA mats to annealing at 90°C, 100°C, and 120°C. The authors report a pronounced increase in the degree of crystallinity, from 2% to 50% after annealing, as evidenced by DSC and wide-angle X-ray scattering (WAXS). The WAXS/XRD intensity profiles of the heat-treated samples detected two sharp diffraction peaks at $2\theta = 16.6°$ and 19.0°, as shown in Figure 5. These peaks are assigned to the (200/110) and (203) planes of the PLLA α'-phase. By contrast, the non-annealed electrospun fibers exhibit a broad amorphous halo. A recent study by Rentero et al. [101] complements these findings and systematically examines thermal post-treatment's impact on electrospun PLA fibers' crystallinity. Their protocol included folding and stacking the electrospun mats, compression-moulding at ~60°C for 3 min under 15 MPa, applying electrodes, and annealing at 100°C for 10 min. This treatment significantly increased crystallinity (e.g., from ~40% to ~60%), raised T_m, and improved piezoelectric response—particularly in fibers with high chiral purity. Moderate, short-time annealing therefore provides an efficient route to increase α-phase content and improve mechanical and functional properties. Prolonged heating (>~60 min) can, however, promote oxidation and chain scission (particularly in high-D-lactide grades); accordingly, shorter protocols or inert atmospheres are advisable. Thus, while ES typically produces highly oriented but predominantly amorphous (α'-rich) PLA networks, post-ES annealing is often necessary to achieve equilibrium α-crystalline states and reduce structural defects.

Other post-processing methods, such as solvent-vapor annealing and constrained thermal treatments, also enhance crystallinity. For instance, annealing PLA composites with 7 wt.% bio fillers at 100°C raised crystallinity to 55% and stiffness by 42%, though over-annealing can cause degradation and molecular weight reduction [102, 103]. Solvent-induced crystallization offers a low-energy approach to increase order within amorphous domains;

exposure to ethanol or acetone vapors plasticizes PLA chains, increases segmental mobility, and promotes α-phase nucleation. For example, ethanol vapor treatment raised crystallinity from 26% to 33%, improving tensile modulus but often reducing elongation at break due to restricted amorphous plasticity [104]. Residual solvent acts as a temporary plasticizer, facilitating chain mobility during crystallization but potentially affecting long-term mechanical stability and biodegradability.

Chemical crosslinking techniques, including peroxide initiation or UV-activated agents, have been applied to electrospun and bulk PLA systems to stabilize crystalline structures. UV-induced crosslinking restricts chain mobility, facilitating stress-induced nucleation within amorphous and crystalline regions, and enhancing the dimensional stability and mechanical strength [105, 106]. However, these crosslinking methods can compromise PLA's inherent biodegradability. Crosslinking increases the polymer's molecular weight and crystallinity, reducing its susceptibility to enzymatic degradation. Consequently, crosslinked PLA may persist longer in natural environments, posing challenges for applications where biodegradation is essential. Therefore, while crosslinking enhances PLA's mechanical properties, it may limit its environmental sustainability [105].

Taken together, ES parameters, additive incorporation, and post-processing treatments represent the three central levers for modulating PLA crystallinity and polymorphism. Their roles, typical outcomes, and unresolved gaps are summarized in Table 3 to provide a concise conceptual framework for subsequent discussion.

3.3 | Future Prospects

Effective control over the crystallization of electrospun PLA fibers hinges on harmonizing additive selection with customized post-processing routines. Researchers can significantly accelerate PLA's naturally slow crystallization by carefully selecting nucleating agents. These can be mineral fillers or bio-based particles that lower the activation energy for crystal growth and promote uniform α- or β-phase domains during ES [107, 108]. When combined with targeted treatments, such as controlled thermal annealing or infrared-assisted preheating, these strategies guide the formation of desirable α-, β-, or even γ-phase domains without excessive energy costs.

Scaling these innovations from single-needle laboratory ES setups to high-throughput manufacturing presents significant challenges. PLA's inherently slow isothermal crystallization requires prolonged residence times or external strategies that accelerate crystallization kinetics—both must be compatible with scalable architectures such as multi-nozzle arrays. Techniques like melt ES and electroblowing have emerged as promising alternatives to solvent-based ES, particularly for industrial-scale production. Melt ES eliminates the need for toxic solvents and enables solvent-free fiber fabrication [107, 109]. For instance, PLA pellets have been directly extruded at speeds of ~1300 g h^{-1} to produce melt-electrospun nonwovens with a basis weight of 45 g m^{-2} [110]. This was achieved under die temperatures of 230°C, hot-air temperatures of 240°C, hot-air pressures of 0.3 MPa, and a die-to-collector distance of 15 cm. However, it demands precise

TABLE 3 | Summary of the three primary strategies for controlling PLA crystallinity and polymorphism in ES, highlighting their main roles, outcomes, and unresolved challenges.

Processing factor	Mechanistic effect	Typical outcome	Key gap
ES parameters (e.g., solution concentration, electric field strength, collector rpm)	Balance between chain entanglement and jet stretching	α-phase favored by strong entanglement; β-like alignment under high strain	Lack of quantitative maps linking parameters to α/β ratios
Additives (e.g., CNC, PDLA, salts)	Heterogeneous nucleation and mobility modulation	CNC/talc promotes α-phase; PDLA yields stereocomplexes	Dispersion limits and ionic-salt mechanisms are not fully resolved
Post-processing treatments (e.g., thermal annealing, solvent vapor)	Lamellar thickening, $\alpha' \rightarrow \alpha$ transition, defect healing	Increased crystallinity, mechanical reinforcement	Trade-offs with degradation and optimal protocols remain unclear

control of polymer melt viscosity, temperature gradients, and flow rates to ensure consistent fiber morphology and prevent thermal degradation. Electroblowing and air-assisted ES, on the other hand, enhance throughput by combining high-voltage fields with pressurized gas streams, which not only accelerate fiber stretching but can also assist in tuning the crystallization behavior of PLA [45]. Industrial-scale electroblowing has demonstrated extrusion rates ranging from 1740 to 3960 g h^{-1} through spinnerets of ~0.25 mm diameter [111]. In these setups, fibers are stretched by high-temperature, high-speed airflows at ~60° angles before cooling and solidification. Additionally, solvent-recovery systems have been explored to reduce environmental impact in traditional solution ES. However, they add considerable complexity to process design and may not be easily integrated with high-throughput fiber alignment mechanisms. Thus, while promising, these advanced ES platforms require careful optimization of crystallization conditions, environmental controls, and equipment design to meet the demands of industrial-scale PLA nanofiber production.

Infrared preheating can be a promising technique to tackle real-time chain entanglement. By locally raising the jet or collector temperature to moderate levels (e.g., 70°C–140°C), infrared irradiation reduces molecular entanglement density, enhances jet stretching, and promotes in-flight crystallite nucleation [27, 112]. Reducing the polymer chain entanglement density, optimizing IR parameters, exposure distance, and pulse duration will be critical to avoid thermal degradation while achieving consistent crystallinity along the fiber length [26, 112].

Complementary to thermal strategies, pulsed electric fields offer another avenue for enhancing molecular orientation and phase ordering. Switching from direct-current to high-frequency pulsed voltages (e.g., 1–10 kHz pulses) can intermittently collapse and rebuild the electrostatic field, driving greater chain alignment without the whipping instabilities of continuous DC [113, 114]. Combined with rotating or patterned collectors or synchronized with plasma modification [115], these approaches can enhance electrospinnability and reach targeted polymorphs before fiber deposition.

Unlocking PLA's full performance potential requires a holistic framework that combines real-time process monitoring—using IR thermography, high-speed imaging, or in situ spectroscopy—with adaptive feedback controls. Machine-learning models trained on process–structure–property datasets can accelerate optimization by revealing the interplay between crystallization kinetics, additive effects, and processing variables.

Building on these principles, we propose a crystallization–scalability framework that bridges recent processing advances for electrospun PLA fibers with industrial scalability, as shown in Figure 6. First, in-flight kinetic control uses IR preheating (70–140°C) techniques and pulsed electric fields (1–10 kHz) to enhance chain orientation and promote targeted nucleation before deposition. Second, polymorph-aware scale-up combines melt-electroblowing, multi-needle ES, and D-lactide zoning to preserve crystalline phase fidelity during high-volume production. Third, closed-loop analytics connect THz-TDS, in-line XRD, IR thermography, and machine learning supervision to enable real-time process optimization.

These combined elements shift the production window toward targeted polymorph control while enabling high-throughput fiber production and integrating sustainability strategies. The framework coordinates factors such as nucleating agents, collector dynamics, annealing, and solvent recovery into a unified framework. In practice, hybrid melt- or solution-based lines equipped with in-line diagnostics can maintain consistent fiber properties. Convolutional neural networks trained on jet imaging and spectral data can predict crystallinity within ±3% and dynamically adjust voltage or IR exposure. Sustainability is reinforced through solvent-free melt processing, green solvent systems with recovery loops, and the adoption of circular feedstocks when performance allows. Functional performance enhancement is achieved by tailoring process parameters to the specific demands of the end application—for example, β-phase piezoelectric sensors benefit from high collector speeds but require annealing to mitigate hydrolytic instability.

4 | Conclusion

Electrospun PLA fibers manifest a complex polymorphic architecture encompassing metastable α', thermodynamically stable α, strain-induced β, and stereocomplex (sc-PLA) domains. Rapid solvent evaporation and sub-ambient processing temperatures during ES kinetically trap PLA in the α' form, yielding defects and limited chain ordering lamellae. Post-spinning isothermal annealing (80°C–120°C) effectively drives the $\alpha' \rightarrow \alpha$ transition, promoting lamellar thickening, defect healing, and improved mechanical performance. Meanwhile, high-strain jet drawing can induce β-phase crystallites that provide fibers with piezoelectric properties yet may compromise ductility and hydrolytic stability. Sc-PLA formation via equimolar PLLA/PDLA blends further enhances melting temperature (T_m ≈220°C–230°C) and mechanical resilience, requiring precise enantiomeric control.

Despite extensive parameter studies—spanning solution concentration, electric field strength, collector dynamics, nucleating-agent incorporation, and post-processing treatments—a cohesive, scalable framework linking polymorphic control, throughput, and real-time feedback remains unresolved. Key challenges include quantifying how β-phase enrichment influences long-term degradation kinetics. Another is assessing the reversibility of ductile α lamellae post-strain, and integrating in situ monitoring (e.g., synchrotron XRD, THz-TDS) into rapid ES platforms. Moreover, trade-offs between energy-intensive annealing, solvent-vapor treatments, and the environmental footprint of crosslinking methods warrant systematic evaluation.

Future research should adopt high-throughput, combinatorial ES experiments—systematically varying solution, field, and additive variables. These experiments should be paired with adaptive feedback controls (e.g., IR thermography, high-speed imaging) and machine-learning models trained on process–structure–property datasets. Such a data-driven, closed-loop approach will accelerate identification of optimal conditions, minimize trial-and-error, and facilitate scale-up from laboratory to industrial multi-nozzle systems. By harmonizing processing kinetics with stereochemical design and post-treatment protocols, this complete approach promises to unlock electrospun PLA fibers' full potential in biomedical scaffolds, filtration membranes, and sustainable tex-

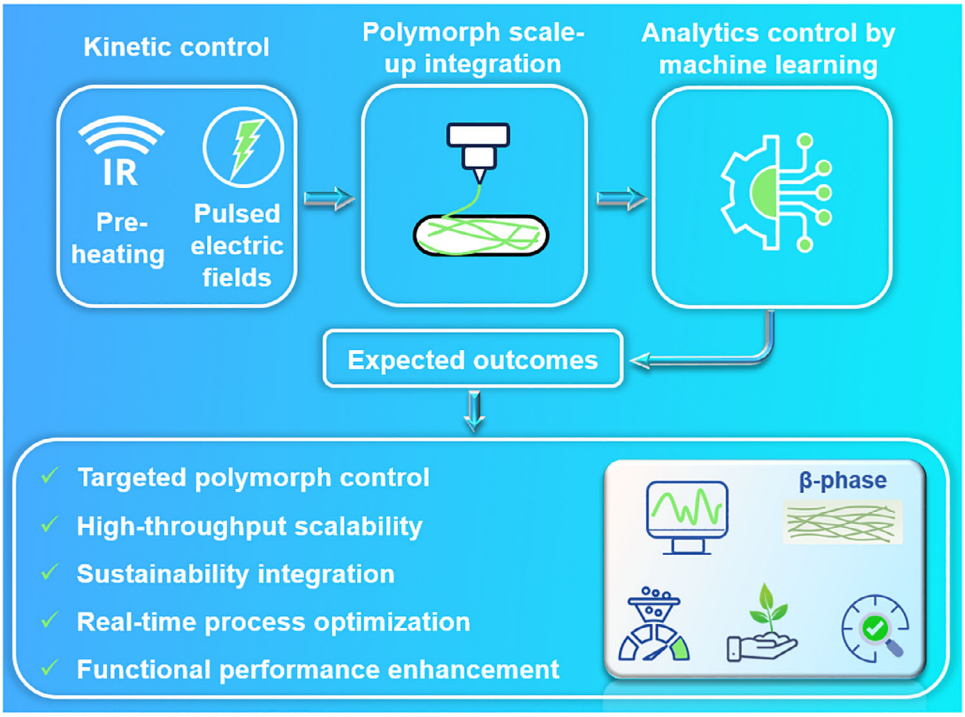

FIGURE 6 | Bridging recent processing developments for electrospun PLA fiber enhancement with industrial scalability, illustrating the incorporation of kinetic control, scale-up, and advanced analytics.

tiles, enabling the production of eco-friendly nanofibers with precisely engineered crystallinity and functionality.

Acknowledgements

Project no. TKP-9-8/PALY-2021 has been implemented with the support provided by the Ministry of Culture and Innovation of Hungary from the National Research, Development, and Innovation Fund, financed under the TKP2021-EGA funding scheme. The research reported in this paper was supported by the National Research, Development and Innovation Office (FK 138501). Kolos Molnár is thankful for the support of the János Bolyai Research Scholarship of the Hungarian Academy of Sciences.

Conflicts of Interest

The authors declare no conflicts of interest.

Data Availability Statement

The authors have nothing to report.

References

1. D. Trivedi, F. Munezero, and N. Rachchh, "Mechanical Characterization of Hybrid Bagasse/Eggshell/E-glass fiber-based Polyester Composite," *Periodica Polytechnica Mechanical Engineering* 68, no. 2 (2024): 130–140, https://doi.org/10.3311/PPme.22963.

2. L. Wu, L. Liu, and J. Zha, "Fabricating Multifunctional PLA Textiles with Advanced Respiratory Detection and Environmental Safety," *Express Polymer Letters* 18 (2024): 1265–1276, https://doi.org/10.3144/expresspolymlett.2024.94.

3. J. Holec, B. Kalous, and C. Brožek, "The Electrospinning of Less Common Polyamides via Direct and Alternating Current," *Express Polymer Letters* 17 (2023): 699–703, https://doi.org/10.3144/expresspolymlett.2023.52.

4. X. Sun, Z. Zhi, B. Hou, W. Li, and G. Liang, "Electrospun Organically Modified Sepiolite/PVDF Coating on Polypropylene Separator to Improve Electrochemical Performance of Lithium-ion Battery," *Express Polymer Letters* 18 (2024): 575–591, https://doi.org/10.3144/expresspolymlett.2024.43.

5. G. Melo and U. Sundararaj, "Influence of Mixed Solvent in the Morphology and Hydrophobicity of Electrospun Polystyrene Porous Fibers," *Macromolecular Rapid Communications* 45, no. 21 (2024): 2400403, https://doi.org/10.1002/marc.202400403.

6. J. Schiffman and C. L. Schauer, "A Review: Electrospinning of Biopolymer Nanofibers and Their Applications," *Polymer Reviews* 48, no. 2 (2008): 317–352, https://doi.org/10.1080/15583720802022182.

7. W. Wu and G. Wu, "Modified Poly(ε-caprolactone) with Larvae Protein Environmentally Friendly Nanofiber: Assessment of Interface Properties and Characterization," *Express Polymer Letters* 18 (2024): 835–850, https://doi.org/10.3144/expresspolymlett.2024.62.

8. Y. Xiong, C. Ni, Y. Chen, et al., "Construction and Performance of PLA-COL@PU-COL@PLA-PU-COL Electrospun Vascular Graft Modified with chitosan/Heparin," *Materials Today Communications* 41 (2024): 111043, https://doi.org/10.1016/j.mtcomm.2024.111043.

9. J. Ye, W. Yu, J. Ge, et al., "Modification of PLA Fibers with Novel Chitosan-based Flame Retardants by Centrifugal Melt Electrospinning," *Materials Today Communications* 38 (2024): 108353, https://doi.org/10.1016/j.mtcomm.2024.108353.

10. S. Pina, J. Oliveira, and R. Reis, "Natural-Based Nanocomposites for Bone Tissue Engineering and Regenerative Medicine: A Review," *Advanced Materials* 27, no. 7 (2015): 1143–1169, https://doi.org/10.1002/adma.201403354.

11. S. Gautam, A. Dinda, and N. Mishra, "Fabrication and Characterization of PCL/Gelatin Composite Nanofibrous Scaffold for Tissue Engineering Applications by Electrospinning Method," *Materials Science and Engineering: C* 33, no. 3 (2013): 1228–1235, https://doi.org/10.1016/j.msec.2012.12.015.

12. B. Sierakowska, P. Radwan, G. Janus, and T. Łysiak, "Preparation and Characterization of Novel Nanofibrous Composites Prepared by Electrospinning as Potential Nerve Guidance Conduits (NGCs)," *Express Polymer Letters* 18 (2024): 819–834, https://doi.org/10.3144/expresspolymlett.2024.61.

13. J. Lo, X. Chen, S. Chen, et al., "Fabrication of Biodegradable PLA-PHBV Medical Textiles via Electrospinning for Healthcare Apparel and Personal Protective Equipment," *Sustainable Chemistry and Pharmacy* 39 (2024): 101536, https://doi.org/10.1016/j.scp.2024.101536.

14. G. Herwig, T. Batt, P. Clement, P. Wick, and R. Rossi, "Sterilization and Filter Performance of Nano- and Microfibrous Facemask Filters – Electrospinning and Restoration of Charges for Competitive Sustainable Alternatives," *Macromolecular Rapid Communications* 46 (2024): 2400867, https://doi.org/10.1002/marc.202400867.

15. S. Keyvani, F. Golbabaei, R. Neisiany, O. Das, M. Pourmand, and S. Kalantary, "Filtration Performance of Biodegradable Electrospun Nanofibrous Membrane for Sub-Micron Particles: A Systematic Review," *Macromolecular Materials and Engineering* 310, no. 3 (2025): 2400323, https://doi.org/10.1002/mame.202400323.

16. M. Mathew, S. Paroly, and S. Athiyanathil, "Biopolymer-based Electrospun Nanofiber Membranes for Smart Food Packaging Applications: A Review," *RSC Advances* 15, no. 27 (2025): 21742–21779, https://doi.org/10.1039/D5RA02348C.

17. Z. Alhulaybi, "Fabrication and Characterization of Poly(lactic acid)-based Biopolymer for Surgical Sutures," *ChemEngineering* 7, no. 5 (2023): 98, https://doi.org/10.3390/chemengineering7050098.

18. A. Trivedi, M. Gupta, and H. Singh, "PLA Based Biocomposites for Sustainable Products: A Review," *Advanced Industrial Engineering Polymer Research* 6, no. 4 (2023): 382–395, https://doi.org/10.1016/j.aiepr.2023.02.002.

19. N. Shekhar and A. Mondal, "Synthesis, Properties, Environmental Degradation, Processing, and Applications of Polylactic Acid (PLA): An Overview," *Polymer Bulletin* 81, no. 13 (2024): 11421–11457, https://doi.org/10.1007/s00289-024-05252-7.

20. A. Rawal, D. Singh, A. Maurya, et al., "Tensile Strength of Continuous and Disordered Fibrous Mats: A Tale of Two-Length Scales," *Macromolecular Rapid Communications* 46 (2025): 2400943, https://doi.org/10.1002/marc.202400943.

21. J. Xue, T. Wu, Y. Dai, and Y. Xia, "Electrospinning and Electrospun Nanofibers: Methods, Materials, and Applications," *Chemical Reviews* 119, no. 8 (2019): 5298–5415, https://doi.org/10.1021/acs.chemrev.8b00593.

22. H. Maleki, R. Semnani Rahbar, M. Saadatmand, and H. Barani, "Physical and Morphological Characterisation of Poly(L-lactide) Acid-based Electrospun Fibrous Structures: Tunning Solution Properties," *Plastics, Rubber and Composites* 47, no. 10 (2018): 438–446, https://doi.org/10.1080/14658011.2018.1532672.

23. H. Maleki, B. Azimi, S. Ismaeilimoghadam, and S. Danti, "Poly(lactic acid)-based Electrospun Fibrous Structures for Biomedical Applications," *Applied Sciences* 12, no. 6 (2022): 3192, https://doi.org/10.3390/app12063192.

24. B. Mao, K. Geers, S. Hu, et al., "Properties of Aligned poly(L-lactic acid) Electrospun Fibers," *Journal of Applied Polymer Science* 132, no. 14 (2015): 41779, https://doi.org/10.1002/app.41779.

25. N. Kalita, S. Bhasney, C. Mudenur, A. Kalamdhad, and V. Katiyar, "End-of-life Evaluation and Biodegradation of Poly(Lactic Acid) (PLA)/Polycaprolactone (PCL)/Microcrystalline Cellulose (MCC) Polyblends Under Composting Conditions," *Chemosphere* 247 (2020): 125875, https://doi.org/10.1016/j.chemosphere.2020.125875.

26. C. Echeverría, I. Limón, A. Muñoz-Bonilla, M. Fernández-García, and D. López, "Development of Highly Crystalline Polylactic Acid with β-crystalline Phase from the Induced Alignment of Electrospun Fibers," *Polymers* 13, no. 17 (2021): 2860, https://doi.org/10.3390/polym13172860.

27. C. Ribeiro, V. Sencadas, C. Costa, J. Gómez Ribelles, and S. Lanceros-Méndez, "Tailoring the Morphology and Crystallinity of Poly(L-lactide acid) Electrospun Membranes," *Science and Technology of Advanced Materials* 12, no. 1 (2011): 015001, https://doi.org/10.1088/1468-6996/12/1/015001.

28. I. Farooq and A. Al-Abduljabbar, "Efficient Production and Experimental Analysis of Bio-based PLA-CA Composite Membranes via Electrospinning for Enhanced Mechanical Performance and Thermal Stability," *Polymers* 17, no. 8 (2025): 1118, https://doi.org/10.3390/polym17081118.

29. G. Stoclet, R. Seguela, C. Vanmansart, C. Rochas, and J. Lefebvre, "WAXS Study of the Structural Reorganization of Semi-crystalline Polylactide under Tensile Drawing," *Polymer* 53, no. 2 (2012): 519–528, https://doi.org/10.1016/j.polymer.2011.11.063.

30. G. Molinari, L. Aliotta, P. Parlanti, M. Gemmi, and A. Lazzeri, "Influence of Moulding Processing on Poly (lactic acid) (PLA) Semi-Crystalline Properties," *Journal of Materials Science* 59, no. 48 (2024): 22344–22362, https://doi.org/10.1007/s10853-024-10497-8.

31. H. Lin, Y. Chen, X. Gao, et al., "Transparent, Heat-resistant, Ductile, and Self-reinforced Polylactide through Simultaneous Formation of Nanocrystals and an Oriented Amorphous Phase," *Macromolecules* 56, no. 6 (2023): 2454–2464, https://doi.org/10.1021/acs.macromol.2c02072.

32. A. Jalali, M. Huneault, and S. Elkoun, "Effect of Molecular Weight on the Nucleation Efficiency of Poly(lactic acid) Crystalline Phases," *Journal of Polymer Research* 24, no. 182 (2017): 11, https://doi.org/10.1007/s10965-017-1337-x.

33. H. Park and C. Hong, "Relationship Between the Stereocomplex Crystallization Behavior and Mechanical Properties of PLLA/PDLA Blends," *Polymers* 13, no. 11 (2021): 1851, https://doi.org/10.3390/polym13111851.

34. M. Samsuri and P. Purnama, "Development of Stereocomplex Polylactide Nanocomposites as an Advanced Class of Biomaterials—A Review," *Polymers* 15, no. 12 (2023): 2730, https://doi.org/10.3390/polym15122730.

35. M. Righetti and E. Tombari, "Crystalline, Mobile Amorphous and Rigid Amorphous Fractions in Poly(L-lactic acid) by TMDSC," *Thermochimica Acta* 522, no. 1 (2011): 118–127, https://doi.org/10.1016/j.tca.2010.12.024.

36. A. Magoń and M. Pyda, "Study of Crystalline and Amorphous Phases of Biodegradable Poly(lactic acid) by Advanced Thermal Analysis," *Polymer* 50, no. 16 (2009): 3967–3973, https://doi.org/10.1016/j.polymer.2009.06.052.

37. W. Limsukon, R. Auras, and T. Smith, "Effects of the Three-phase Crystallization Behavior on the Hydrolysis of Amorphous and Semicrystalline Poly(lactic acid)s, ACS Appl," *Polymer Material* 3, no. 11 (2021): 5920–5931, https://doi.org/10.1021/acsapm.1c01080.

38. A. Sangroniz, A. Chaos, M. Iriarte, J. del Río, J. Sarasua, and A. Etxeberria, "Influence of the Rigid Amorphous Fraction and Crystallinity on Polylactide Transport Properties," *Macromolecules* 51, no. 11 (2018): 3923–3931, https://doi.org/10.1021/acs.macromol.8b00833.

39. J. del Río, A. Etxeberria, N. López-Rodríguez, E. Lizundia, and J. Sarasua, "A PALS Contribution to the Supramolecular Structure of Poly(l-lactide)," *Macromolecules* 43, no. 10 (2010): 4698–4707, https://doi.org/10.1021/ma902247y.

40. J. Sarasua, N. Rodríguez, A. Arraiza, and E. Meaurio, "Stereoselective Crystallization and Specific Interactions in Polylactides," *Macromolecules* 38, no. 20 (2005): 8362–8371, https://doi.org/10.1021/ma051266z.

41. P. Klonos, N. Bikiaris, P. Barmpalexis, and A. Kyritsis, "Segmental Mobility in Linear Polylactides of Various Molecular Weights," *Polymer* 305 (2024): 127177, https://doi.org/10.1016/j.polymer.2024.127177.

42. A. Afifi, H. Yamane, and Y. Kimura, "Effect of Polymer Molecular Weight on the Electrospinning of Polylactides in Entangled and Aligned fiber Forms," *Sen'i Gakkaishi* 66, no. 2 (2010): 35–42, https://doi.org/10.2115/fiber.66.35.

43. S. Li, R. Lv, H. Liu, B. Na, H. Zhou, and L. Ge, "Uniform High-Molecular-Weight Polylactide Nanofibers Electrospun from a Solution Below its Entanglement Concentration," *Journal of Applied Polymer Science* 134, no. 21 (2017), https://doi.org/10.1002/app.44853.

44. A. El Aferni, M. Guettari, M. Kamli, T. Tajouri, and A. Ponton, "A Structural Study of a Polymer-surfactant System in Dilute and Entangled Regime: Effect of High Concentrations of Surfactant and Polymer Molecular Weight," *Journal of Molecular Structure* 1199 (2020): 127052, https://doi.org/10.1016/j.molstruc.2019.127052.

45. K. Abdullah and K. Molnár, "A Novel Air-flow Electrospinning Setup for Controlling fiber Distribution and Morphology," *Solid State Phenomena* 371 (2025): 37–44, https://doi.org/10.4028/p-piso85.

46. P. De Santis and A. Kovacs, "Molecular Conformation of Poly(S-Lactic Acid)," *Biopolymers* 6, no. 3 (1968): 299–306, https://doi.org/10.1002/bip.1968.360060305.

47. L. Jiang, T. Shen, P. Xu, et al., "Crystallization Modification of Poly(lactide) by Using Nucleating Agents and Stereocomplexation," *e-Polymers* 16, no. 1 (2016): 1–13, https://doi.org/10.1515/epoly-2015-0179.

48. K. Wasanasuk, K. Tashiro, M. Hanesaka, et al., "Crystal Structure Analysis of Poly(l-lactic acid) α Form on the Basis of the 2-dimensional Wide-angle Synchrotron X-ray and Neutron Diffraction Measurements," *Macromolecules* 44, no. 16 (2011): 6441–6452, https://doi.org/10.1021/ma2006624.

49. J. Zhang, K. Tashiro, H. Tsuji, and A. Domb, "Disorder-to-order Phase Transition and Multiple Melting Behavior of Poly(l-lactide) Investigated by Simultaneous Measurements of WAXD and DSC," *Macromolecules* 41, no. 4 (2008): 1352–1357, https://doi.org/10.1021/ma0706071.

50. M. Puchalski, S. Kwolek, G. Szparaga, M. Chrzanowski, and I. Krucińska, "Investigation of the Influence of PLA Molecular Structure on the Crystalline Forms (α' and α) and Mechanical Properties of Wet Spinning Fibres," *Polymers* 9, no. 1 (2017): 18, https://doi.org/10.3390/polym9010018.

51. T. Kawai, N. Rahman, G. Matsuba, et al., "Crystallization and Melting Behavior of Poly (l-lactic acid)," *Macromolecules* 40, no. 26 (2007): 9463–9469, https://doi.org/10.1021/ma070082c.

52. K. Shi, G. Liu, H. Sun, B. Yang, and Y. Weng, "Effect of Biomass as Nucleating Agents on Crystallization Behavior of Polylactic Acid," *Polymers* 14, no. 20 (2022): 4305, https://doi.org/10.3390/polym14204305.

53. W. Hoogsteen, A. Postema, A. Pennings, G. Ten Brinke, and P. Zugenmaier, "Crystal Structure, Conformation and Morphology of Solution-spun Poly(L-lactide) Fibers," *Macromolecules* 23, no. 2 (1990): 634–642, https://doi.org/10.1021/ma00204a041.

54. H. Wang, J. Zhang, and K. Tashiro, "Phase Transition Mechanism of Poly(l-lactic acid) among the α, δ, and β Forms on the Basis of the Reinvestigated Crystal Structure of the β Form," *Macromolecules* 50, no. 8 (2017): 3285–3300, https://doi.org/10.1021/acs.macromol.7b00272.

55. S. Xu, J. Zhou, and P. Pan, "Strain-induced Multiscale Structural Evolutions of Crystallized Polymers: From Fundamental Studies to Recent Progresses," *Progress in Polymer Science* 140 (2023): 101676, https://doi.org/10.1016/j.progpolymsci.2023.101676.

56. K. Ramadan, D. Sameoto, and S. Evoy, "A Review of Piezoelectric Polymers as Functional Materials for Electromechanical Transducers," *Smart Materials and Structures* 23, no. 3 (2014): 033001, https://doi.org/10.1088/0964-1726/23/3/033001.

57. B. Lotz, "*Crystal Polymorphism and Morphology of Polylactides*," in *Synthesis, Structure and Properties of Poly(lactic acid)*, Eds: M. L. Di Lorenzo and R. Androsch (Springer International Publishing, 2018): 273–302, https://doi.org/10.1007/12_2016_15.

58. H. Tsuji, "Poly(lactic acid) stereocomplexes: A decade of progress," *Advanced Drug Delivery Reviews* 107 (2016): 97–135, https://doi.org/10.1016/j.addr.2016.04.017.

59. M. Sun, S. Lu, P. Zhao, Z. Feng, M. Yu, and K. Han, "Scalable Preparation of Complete Stereo-complexation Polylactic Acid fiber and Its Hydrolysis Resistance," *Molecules (Basel, Switzerland)* 27, no. 21 (2022): 7654, https://doi.org/10.3390/molecules27217654.

60. X. Wei, R. Bao, Z. Cao, et al., "Greatly Accelerated Crystallization of Poly(lactic acid): Cooperative Effect of Stereocomplex Crystallites and Polyethylene Glycol," *Colloid and Polymer Science* 292, no. 1 (2014): 163–172, https://doi.org/10.1007/s00396-013-3067-x.

61. H. Tsuji, M. Nakano, M. Hashimoto, K. Takashima, S. Katsura, and A. Mizuno, "Electrospinning of Poly(lactic acid) Stereocomplex Nanofibers," *Biomacromolecules* 7, no. 12 (2006): 3316–3320, https://doi.org/10.1021/bm060786e.

62. C. Alemán, B. Lotz, and J. Puiggali, "Crystal Structure of the α-form of Poly(l-lactide)," *Macromolecules* 34, no. 14 (2001): 4795–4801, https://doi.org/10.1021/ma001630o.

63. M. Righetti, M. Gazzano, M. Di Lorenzo, and R. Androsch, "Enthalpy of Melting of α'- and α-crystals of Poly(l-lactic acid)," *European Polymer Journal* 70 (2015): 215–220, https://doi.org/10.1016/j.eurpolymj.2015.07.024.

64. D. Sawai, K. Takahashi, A. Sasashige, T. Kanamoto, and S. Hyon, "Preparation of Oriented β-form Poly(l-lactic acid) by Solid-state Coextrusion: Effect of Extrusion Variables," *Macromolecules* 36, no. 10 (2003): 3601–3605, https://doi.org/10.1021/ma030050z.

65. L. Cartier, T. Okihara, Y. Ikada, H. Tsuji, J. Puiggali, and B. Lotz, "Epitaxial Crystallization and Crystalline Polymorphism of Polylactides," *Polymer* 41, no. 25 (2000): 8909–8919, https://doi.org/10.1016/S0032-3861(00)00234-2.

66. Z. Zhu, Y. Bian, X. Zhang, R. Zeng, and B. Yang, "Study on the Crystallization Behavior and Conformation Adjustment Scale of Poly(lactic acid) in the Terahertz Frequency Range," *Physical Chemistry Chemical Physics* 25, no. 12 (2023): 8472–8481, https://doi.org/10.1039/D3CP00208J.

67. Z. Zhu, Y. Bian, X. Zhang, R. Zeng, and B. Yang, "Study of Crystallinity and Conformation of Poly(lactic acid) by Terahertz Spectroscopy," *Analytical Chemistry* 94, no. 31 (2022): 11104–11111, http://doi.org/10.1021/acs.analchem.2c02652.

68. J. Zhang, D. Yan, J. Xu, H. Huang, J. Lei, and Z. Li, "Highly Crystallized Poly (lactic acid) under High Pressure," *AIP Advances* 2, no. 4 (2012), https://doi.org/10.1063/1.4769351.

69. P. Gao and D. Masato, "The Effects of Nucleating Agents and Processing on the Crystallization and Mechanical Properties of Polylactic Acid: A Review," *Micromachines* 15, no. 6 (2024): 776, https://doi.org/10.3390/mi15060776.

70. C. Zhou, H. Li, W. Zhang, et al., "Thermal Strain-induced Cold Crystallization of Amorphous Poly(lactic acid)," *CrystEngComm* 18, no. 18 (2016): 3237–3246, https://doi.org/10.1039/C6CE00464D.

71. H. Lu, S. Kazarian, and H. Sato, "Simultaneous Visualization of Phase Separation and Crystallization in PHB/PLLA Blends with in Situ ATR-FTIR Spectroscopic Imaging," *Macromolecules* 53, no. 20 (2020): 9074–9085, https://doi.org/10.1021/acs.macromol.0c00713.

72. M. Wang, Y. Cai, B. Zhao, and P. Zhu, "Time-Resolved Study of Nanomorphology and Nanomechanic Change of Early-Stage Mineralized Electrospun Poly(lactic acid) Fiber by Scanning Electron Microscopy, Raman Spectroscopy and Atomic Force Microscopy," *Nanomaterials* 7, no. 8 (2017): 223, https://doi.org/10.3390/nano7080223.

73. A. Frone, D. Panaitescu, I. Chiulan, et al., "The Effect of Cellulose Nanofibers on the Crystallinity and Nanostructure of Poly(lactic acid) Composites," *Journal of Materials Science* 51, no. 21 (2016): 9771–9791, https://doi.org/10.1007/s10853-016-0212-1.

74. Y. Zhu, C. Li, and P. Cebe, "Poly(lactides) co-electrospun with Carbon Nanotubes: Thermal and Cell Culture Properties," *European Polymer Journal* 75 (2016): 565–576, https://doi.org/10.1016/j.eurpolymj.2016.01.014.

75. S. Iannace, A. Maffezzoli, G. Leo, and L. Nicolais, "Influence of Crystal and Amorphous Phase Morphology on Hydrolytic Degradation of PLLA Subjected to Different Processing Conditions," *Polymer* 42, no. 8 (2001): 3799–3807, https://doi.org/10.1016/S0032-3861(00)00744-8.

76. C. Schick, A. Wurm, and A. Mohammed, "Formation and Disappearance of the Rigid Amorphous Fraction in Semicrystalline Polymers Revealed from Frequency Dependent Heat Capacity," *Thermochimica*

Acta 396, no. 1 (2003): 119–132, https://doi.org/10.1016/S0040-6031(02)00526-9.

77. K. Abdullah and K. Molnár, "The Influence of in Vitro Degradation on the Properties of Polylactic Acid Electrospun fiber Mats," *Fibers* 13, no. 1 (2025): 1–20, https://doi.org/10.3390/fib13010001.

78. M. Smyth, V. Poursorkhabi, A. Mohanty, S. Gregori, and M. Misra, "Electrospinning Highly Oriented and Crystalline Poly(lactic acid) fiber Mats," *Journal of Materials Science* 49, no. 6 (2014): 2430–2441, https://doi.org/10.1007/s10853-013-7899-z.

79. R. Kaur and I. Chauhan, "Biodegradable Plastics: Mechanisms of Degradation and Generated Bio Microplastic Impact on Soil Health," *Biodegradation* 35, no. 6 (2024): 863–892, https://doi.org/10.1007/s10532-024-10092-3.

80. A. Leonés, L. Peponi, M. Lieblich, R. Benavente, and S. Fiori, "In Vitro Degradation of Plasticized PLA Electrospun fiber Mats: Morphological, Thermal and Crystalline Evolution," *Polymers* 12, no. 12 (2020): 2975, https://doi.org/10.3390/polym12122975.

81. M. Giełdowska, M. Puchalski, S. Sztajnowski, and I. Krucińska, "Evolution of the Molecular and Supramolecular Structures of PLA during the Thermally Supported Hydrolytic Degradation of Wet Spinning Fibers," *Macromolecules* 55, no. 22 (2022): 10100–10112, https://doi.org/10.1021/acs.macromol.2c01778.

82. S. Lomakin, Y. Mikheev, S. Usachev, et al., "Evaluation and Modeling of Polylactide Photodegradation under Ultraviolet Irradiation: Bio-based Polyester Photolysis Mechanism," *Polymers* 16, no. 7 (2024): 985, https://doi.org/10.3390/polym16070985.

83. S. Lv, Y. Zhang, and H. Tan, "Thermal and Thermo-oxidative Degradation Kinetics and Characteristics of Poly (lactic acid) and Its Composites," *Waste Management* 87 (2019): 335–344, https://doi.org/10.1016/j.wasman.2019.02.027.

84. O. Ero-Phillips, M. Jenkins, and A. Stamboulis, "Tailoring Crystallinity of Electrospun PLLA Fibres by Control of Electrospinning Parameters," *Polymers* 4, no. 3 (2012): 1331–1348, https://doi.org/10.3390/polym4031331.

85. L. Xia, L. Lu, and Y. Liang, "Preparation and Characterization of Poly(lactic acid) Micro- and Nanofibers Fabricated by Centrifugal Spinning," *Fibers and Polymers* 21, no. 7 (2020): 1422–1429, https://doi.org/10.1007/s12221-020-9993-6.

86. K. Abdullah and K. Molnár, "Current Trends and Future Prospects of Integrating Electrospinning with 3D Printing Techniques for Mimicking Bone Extracellular Matrix Scaffolds," *Journal of Polymer Science* 63, no. 6 (2025): 1481–1504, https://doi.org/10.1002/pol.20241010.

87. A. Kotrotsos, P. Yiallouros, and V. Kostopoulos, "Fabrication and Characterization of Polylactic Acid Electrospun Scaffolds Modified with Multi-walled Carbon Nanotubes and Hydroxyapatite Nanoparticles," *Biomimetics* 5, no. 3 (2020): 43, https://doi.org/10.3390/biomimetics5030043.

88. M. Mushtaq, M. Wasim, M. Naeem, et al., "Composite of PLA Nanofiber and Hexadecyl Trimethyl-Ammonium Chloride-modified Montmorillonite Clay: Fabrication and Morphology," *Coatings* 10, no. 5 (2020): 484, https://doi.org/10.3390/coatings10050484.

89. A. Leonés, V. Salaris, A. Mujica-Garcia, et al., "PLA Electrospun Fibers Reinforced with Organic and Inorganic Nanoparticles: A Comparative Study," *Molecules (Basel, Switzerland)* 26, no. 16 (2021): 4925, https://doi.org/10.3390/molecules26164925.

90. J. Zhao, T. Li, H. Sun, et al., "Regulated Crystallization and Piezoelectric Properties of Bio-based Poly(L-lactic acid)/Diatomite Composite Fibers by Electrospinning," *Advanced Composites and Hybrid Materials* 7, no. 6 (2024): 218, https://doi.org/10.1007/s42114-024-01034-x.

91. C. Odili, O. Gbenebour, O. Olanrewaju, T. Badaru, and S. Adeosun, "Physiochemical Performance of Electrospun PLA-lignin and PVA-lignin," *Journal of Materials Science: Materials in Engineering* 20, no. 1 (2025): 10, https://doi.org/10.1186/s40712-025-00218-7.

92. S. Karpova, A. Olkhov, I. Varyan, et al., "Electrospun Polylactide—Poly(ε-Caprolactone) Fibers: Structure Characterization and Segmental Dynamic Response," *Polymers* 16, no. 10 (2024): 1307, https://doi.org/10.3390/polym16101307.

93. Y. Cheng, Z. Jiao, M. Li, et al., "A New Class of Nucleating Agents for Poly(L-lactic acid): Environmentally-friendly Metal Salts with Biomass-Derived Ligands and Advanced Nucleation Ability," *International Journal of Biological Macromolecules* 225 (2023): 1599–1606, https://doi.org/10.1016/j.ijbiomac.2022.11.216.

94. L. Aliotta, P. Cinelli, M. Coltelli, M. Righetti, M. Gazzano, and A. Lazzeri, "Effect of Nucleating Agents on Crystallinity and Properties of Poly (lactic acid) (PLA)," *European Polymer Journal* 93 (2017): 822–832, https://doi.org/10.1016/j.eurpolymj.2017.04.041.

95. R. Scaffaro and F. Lopresti, "Properties-morphology Relationships in Electrospun Mats Based on Polylactic Acid and Graphene Nanoplatelets," *Composites Part A: Applied Science and Manufacturing* 108 (2018): 23–29, https://doi.org/10.1016/j.compositesa.2018.02.026.

96. C. Ouyang, H. Zhang, Y. Zhu, J. Zhao, H. Ren, and H. Zhai, "Lignin-containing Cellulose Nanocrystals Enhanced Electrospun Polylactic Acid-based Nanofibrous Mats: Strengthen and Toughen," *International Journal of Biological Macromolecules* 280 (2024): 135617, https://doi.org/10.1016/j.ijbiomac.2024.135617.

97. R. Kumar Singla, S. N. Maiti, and A. Kumar Ghosh, "Crystallization, Morphological, and Mechanical Response of Poly(lactic acid)/Lignin-based Biodegradable Composites," *Polymer-Plastics Technology and Engineering* 55, no. 5 (2016): 475–485, https://doi.org/10.1080/03602559.2015.1098688.

98. Q. Shi, C. Zhou, Y. Yue, W. Guo, Y. Wu, and Q. Wu, "Mechanical Properties and in Vitro Degradation of Electrospun Bio-Nanocomposite Mats from PLA and Cellulose Nanocrystals," *Carbohydrate Polymers* 90, no. 1 (2012): 301–308, https://doi.org/10.1016/j.carbpol.2012.05.042.

99. S. Sasaki and T. Asakura, "Helix Distortion and Crystal Structure of the α-Form of Poly(l -lactide)," *Macromolecules* 36, no. 22 (2003): 8385–8390, https://doi.org/10.1021/ma0348674.

100. N. Cuong, S. Barrau, M. Dufay, et al., "On the Nanoscale Mapping of the Mechanical and Piezoelectric Properties of Poly (l-lactic Acid) Electrospun Nanofibers," *Applied Sciences* 10, no. 2 (2020): 652, https://doi.org/10.3390/app10020652.

101. C. Rentero, H. Amorín, R. Jiménez, M. Mosquera, and V. Sessini, "Key Factors Affecting the Piezoelectric Response of Poly-L-lactic Acid Electrospun Fibers," *Polymer* 325 (2025): 128286, https://doi.org/10.1016/j.polymer.2025.128286.

102. S. Nauman, G. Lubineau, and H. Alharbi, "Post Processing Strategies for the Enhancement of Mechanical Properties of Enms (electrospun nanofibrous membranes): A Review," *Membranes* 11, no. 1 (2021): 39, https://doi.org/10.3390/membranes11010039.

103. H. Simmons, P. Tiwary, J. Colwell, and M. Kontopoulou, "Improvements in the Crystallinity and Mechanical Properties of PLA by Nucleation and Annealing," *Polymer Degradation and Stability* 166 (2019): 248–257, https://doi.org/10.1016/j.polymdegradstab.2019.06.001.

104. D. Vadas, Z. Nagy, I. Csontos, G. Marosi, and K. Bocz, "Effects of Thermal Annealing and Solvent-induced Crystallization on the Structure and Properties of Poly(lactic acid) Microfibres Produced by High-speed Electrospinning," *Journal of Thermal Analysis and Calorimetry* 142, no. 2 (2020): 581–594, https://doi.org/10.1007/s10973-019-09191-8.

105. M. Bednarek, K. Borska, and P. Kubisa, "Crosslinking of Polylactide by High Energy Irradiation and Photo-curing," *Molecules (Basel, Switzerland)* 25, no. 21 (2020): 4919, https://doi.org/10.3390/molecules25214919.

106. F. Chen, G. Hochleitner, T. Woodfield, J. Groll, P. Dalton, and B. Amsden, "Additive Manufacturing of a Photo-cross-linkable Polymer via Direct Melt Electrospinning Writing for Producing High Strength Structures," *Biomacromolecules* 17, no. 1 (2016): 208–214, https://doi.org/10.1021/acs.biomac.5b01316.

107. Y. Liu, S. Jiang, W. Yan, et al., "Crystallization Morphology Regulation on Enhancing Heat Resistance of Polylactic Acid," *Polymers* 12, no. 7 (2020): 1563, https://doi.org/10.3390/polym12071563.

108. A. El-Hadi, S. Mohan, F. Davis, and G. Mitchell, "Enhancing the Crystallization and Orientation of Electrospinning Poly (lactic acid) (PLLA) by Combining with Additives," *Journal of Polymer Research* 21, no. 12 (2014): 605, https://doi.org/10.1007/s10965-014-0605-2.

109. K. Koenig, F. Langensiepen, and G. Seide, "Pilot-scale Production of Polylactic Acid Nanofibers by Melt Electrospinning," *e-Polymers* 20, no. 1 (2020): 233–241, https://doi.org/10.1515/epoly-2020-0030.

110. Y. Zhao, S. Zhang, D. Yan, J. Ming, X. Wang, and X. Ning, "Combination Strategy of Melt-blowing and Breath-figure Enabling Scale-up Production of Hierarchically Structured Polylactic Acid (PLA) Nonwovens for Durable and Efficient Air Filtration," *Advanced Fiber Materials* 7, no. 2 (2025): 620–632, https://doi.org/10.1007/s42765-025-00511-2.

111. G. Liu, J. Guan, X. Wang, J. Yu, and B. Ding, "Polylactic Acid (PLA) Melt-blown Nonwovens with Superior Mechanical Properties," *ACS Sustainable Chemistry & Engineering* 11, no. 10 (2023): 4279–4288, https://doi.org/10.1021/acssuschemeng.3c00159.

112. E. Meaurio, N. López-Rodríguez, and J. Sarasua, "Infrared Spectrum of Poly(l-lactide): Application to Crystallinity Studies," *Macromolecules* 39, no. 26 (2006): 9291–9301, https://doi.org/10.1021/ma061890r.

113. A. Mirek, P. Korycka, M. Grzeczkowicz, and D. Lewińska, "Polymer Fibers Electrospun Using Pulsed Voltage," *Materials & Design* 183 (2019): 108106, https://doi.org/10.1016/j.matdes.2019.108106.

114. A. Bartkowiak, M. Grzeczkowicz, and D. Lewińska, "The Effects of Pulsed Electrospinning Process Variables on the Size of Polymer Fibers Established with a 23 Factorial Design," *Polymers* 16, no. 16 (2024): 2352, https://doi.org/10.3390/polym16162352.

115. F. Rezaei, A. Nikiforov, R. Morent, and N. De Geyter, "Plasma Modification of Poly Lactic Acid Solutions to Generate High Quality Electrospun PLA Nanofibers," *Scientific Reports* 8, no. 1 (2018): 2241, https://doi.org/10.1038/s41598-018-20714-5.